

Demonstration and validation of a hybrid vibration prediction tool for railway induced vibration

Pieter Reumers¹, Geert Lombaert¹, Geert Degrande¹, Evangelos Ntotsios², David Thompson², Brice Nélain³, Sylvain Barcet³, Pascal Bouvet³, Bernd Fröhling⁴, Andreas Nuber⁴

¹KU Leuven, Department of Civil Engineering, Kasteelpark Arenberg 40, B-3001 Leuven, Belgium

²University of Southampton, ISVR, Highfield, Southampton SO17 1BJ, United Kingdom

³Vibratec, 28 Chemin du petit bois, F-69131, Ecully, France

⁴Wölfel Engineering GmbH + Co. KG, Max-Planck Strasse 15, D-97204 Höchberg, Germany

KEYWORDS: railway induced vibration, hybrid prediction model, software tool, experimental validation

ABSTRACT

Although rail is a sustainable and climate-friendly mode of transport, noise and vibration remain particular environmental concerns. Within SILVARSTAR, a two-year collaborative project funded under the Shift2Rail Joint Undertaking in Horizon 2020, the aim is to develop validated software tools to assess the noise and vibration environmental impact of new railway lines or the extension of existing lines. One of two major objectives is the development of a hybrid vibration prediction tool for railway induced vibration incorporating widely accepted solution methods and standards. In order to keep the computational effort low, the soil impedance and track-soil transfer functions are pre-computed for a large number of cases and stored in a numerical database. Additionally, the vibration velocity level is predicted using a low speed approximation, which disregards the Doppler effect. Incoherent axle loads are also assumed. This paper demonstrates the use of the vibration prediction tool for tracks at grade and in tunnels; results are validated with state-of-the-art numerical models.

INTRODUCTION

The aim of the project SILVARSTAR is the development of efficient noise and vibration prediction tools for railways based on widely accepted solution methods and standards. This paper presents a demonstration and validation of the hybrid vibration prediction tool developed within the project. The hybrid framework originates from the empirical procedure for Detailed Vibration Assessment proposed by the Federal Railroad Administration (FRA) and the Federal Transit Administration (FTA) [1, 2].

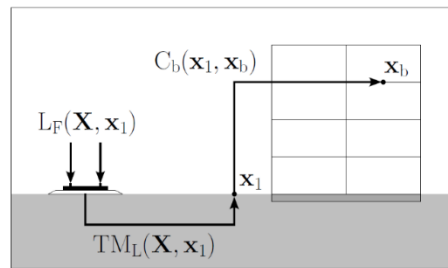


Fig. 1 Hybrid framework based on the FRA and FTA guidelines.

The vibration velocity level $L_v(\mathbf{x}_b)$ in each frequency band at a receiver \mathbf{x}_b inside a building is expressed as the sum of a force density $L_F(\mathbf{X}, \mathbf{x}_1)$, a line source transfer mobility $TM_L(\mathbf{X}, \mathbf{x}_1)$ and a building correction factor $C_b(\mathbf{x}_1, \mathbf{x}_b)$:

$$L_v(\mathbf{x}_b) = L_F(\mathbf{X}, \mathbf{x}_1) + TM_L(\mathbf{X}, \mathbf{x}_1) + C_b(\mathbf{x}_1, \mathbf{x}_b) \quad (1)$$

where \mathbf{x}_1 is the position of a receiver in the free field and \mathbf{X} is the set of source positions along the track (Fig. 1). Each term in Eq. (1) can be represented by either numerical predictions or empirical data. Omitting the building correction factor $C_b(\mathbf{x}_1, \mathbf{x}_b)$ from Eq. (1), this results in two hybrid prediction schemes:

Hybrid scheme 1 - predicted force density $L_F^{\text{NUM}}(\mathbf{X})$ combined with a measured line source transfer mobility $TM_L^{\text{EXP}}(\mathbf{X}, \mathbf{x}_1)$:

$$L_v^{\text{HYB}}(\mathbf{x}_1) = L_F^{\text{NUM}}(\mathbf{X}) + TM_L^{\text{EXP}}(\mathbf{X}, \mathbf{x}_1) \quad (2a)$$

where the predicted force density $L_F^{\text{NUM}}(\mathbf{X})$ is computed directly from the dynamic axle loads. Alternatively, the vibration velocity level can be predicted as:

$$\begin{aligned} L_v^{\text{HYB}}(\mathbf{x}_1) &= L_F^{\text{NUM}}(\mathbf{X}, \mathbf{x}_1) + TM_L^{\text{EXP}}(\mathbf{X}, \mathbf{x}_1) \\ &= L_v^{\text{NUM}}(\mathbf{x}_1) - TM_L^{\text{NUM}}(\mathbf{X}, \mathbf{x}_1) + TM_L^{\text{EXP}}(\mathbf{X}, \mathbf{x}_1) \end{aligned} \quad (2b)$$

where the force density $L_F^{\text{NUM}}(\mathbf{X}, \mathbf{x}_1)$ is computed indirectly as the difference between the vibration velocity level $L_v^{\text{NUM}}(\mathbf{x}_1)$ and line source transfer mobility $TM_L^{\text{NUM}}(\mathbf{X}, \mathbf{x}_1)$. When a low speed approximation is used, $L_F^{\text{NUM}}(\mathbf{X})$ and $L_F^{\text{NUM}}(\mathbf{X}, \mathbf{x}_1)$ match relatively well [3, 4].

Hybrid scheme 2 - measured force density $L_F^{\text{EXP}}(\mathbf{X}, \mathbf{x}_1)$ combined with a predicted line source transfer mobility $TM_L^{\text{NUM}}(\mathbf{X}, \mathbf{x}_1)$:

$$\begin{aligned} L_v^{\text{HYB}}(\mathbf{x}_1) &= L_F^{\text{EXP}}(\mathbf{X}, \mathbf{x}_1) + TM_L^{\text{NUM}}(\mathbf{X}, \mathbf{x}_1) \\ &= L_v^{\text{EXP}}(\mathbf{x}_1) - TM_L^{\text{EXP}}(\mathbf{X}, \mathbf{x}_1) + TM_L^{\text{NUM}}(\mathbf{X}, \mathbf{x}_1) \end{aligned} \quad (3)$$

where the measured force density $L_F^{\text{EXP}}(\mathbf{X}, \mathbf{x}_1)$ is estimated as the difference between the measured vibration velocity level $L_v^{\text{EXP}}(\mathbf{x}_1)$ and line source transfer mobility $TM_L^{\text{EXP}}(\mathbf{X}, \mathbf{x}_1)$.

These hybrid schemes, together with a fully numerical prediction scheme, are implemented in the vibration prediction tool that consists of a computational core, a numerical and experimental database, and a Graphical User Interface (GUI) to input data and visualize results. The tool is integrated in the noise mapping software IMMI, providing an interface with Geographical Information Systems (GIS).

The computational core uses a 2.5D model [5, 6] to calculate the track receptance in the wavenumber-frequency domain. To speed up computations, a numerical database of pre-computed soil impedance and track-soil transfer functions is created for several homogeneous and layered soil profiles, track widths ranging from 3 m to 12 m for tracks at grade, and tunnel diameters between 4 m and 16 m and depths between 10 m and 20 m [7]. State-of-the-art numerical models MOTIV [8, 9] and TRAFFIC [10] are used to validate the computational core and the modelling assumptions: low speed approximation (disregarding the Doppler effect) and incoherent axle loads. The validation is presented in [4, 11] for several case histories.

An experimental database is embedded in the vibration prediction tool, containing train passages, track-soil transfer functions and building correction factors measured at several well-documented sites across Europe [7]. The database can be extended by the user with project specific data to perform transposition from one situation into another.

This paper considers two case histories to demonstrate and validate the hybrid vibration prediction tool: (1) a slab track in a tunnel and (2) a ballasted track at grade in Lincent (Belgium). For the second case, experimental data are used to demonstrate and validate the hybrid prediction schemes.

SLAB TRACK IN A TUNNEL

Case description

A concrete tunnel with outer diameter 6 m and wall thickness 0.3 m is embedded at a depth of 15 m in soft, medium and stiff soil (properties in Table 1). The tunnel properties are summarized in Table 2. At the tunnel invert, a slab track with properties listed in Table 3 is installed. An extra mass of 1200 kg/m is added to the mass of the slab to account for any material between the slab and the tunnel invert. The track centre is positioned symmetrically with respect to the centre of the tunnel. In the vibration prediction tool, the tunnel impedance and tunnel-soil transfer functions are imported from the numerical database [7]. These data were pre-computed with MOTIV. The tunnel impedance is subsequently coupled to the track model.

Table 1 Dynamic soil characteristics: shear wave velocity C_s , dilatational wave velocity C_p , density ρ , and material damping ratios β_s and β_p for shear and dilatational deformation.

Soil type	C_s [m/s]	C_p [m/s]	ρ [kg/m ³]	β_s [-]	β_p [-]
Soft	100	200	1800	0.025	0.025
Medium	200	400	1800	0.025	0.025
Stiff	400	800	1800	0.025	0.025

Table 2 Tunnel properties.

Outer diameter	$D_t = 6$ m
Wall thickness	$t_t = 0.3$ m
Young's modulus	$E_t = 50$ GPa
Density	$\rho_t = 2500$ kg/m ³
Poisson's ratio	$\nu_t = 0.2$
Damping loss factor	$\eta_t = 0.02$

Table 3 Properties of the slab track in the tunnel.

Rail UIC60	Rail positions	$l_1 = l_2 = 0.72$ m
	Cross-sectional area	$A_r = 76.70 \times 10^{-4}$ m ²
	Second moment of area	$I_r = 3057.1 \times 10^{-8}$ m ⁴
	Young's modulus	$E_r = 210$ GPa
	Damping loss factor	$\eta_r = 0.01$
	Density	$\rho_r = 7850$ kg/m ³
Rail pad	Spacing	$d = 0.65$ m
	Stiffness	$k_{rp} = 120 \times 10^6$ N/m
	Damping loss factor	$\eta_{rp} = 0.15$
Slab	Width	$b_{sl} = 3.45$ m
	Thickness	$h_{sl} = 0.30$ m
	Young's modulus	$E_{sl} = 30$ GPa
	Damping loss factor	$\eta_{sl} = 0.015$
	Mass per unit length	$\rho_{sl}A_{sl} = 2520$ kg/m
	Extra mass per unit length	$m = 1200$ kg/m

The track unevenness is determined from measurements on a normally maintained slab track [7]. The one-sided PSD of the track unevenness is compared to the FRA curves in Fig. 2. For short wavelengths, the track quality is close to FRA class 2 track quality; the track unevenness is lower compared to FRA class 6 at longer wavelengths.

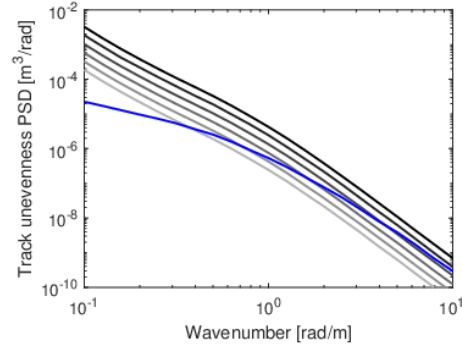


Fig. 2 One-sided PSD of the track unevenness for FRA track quality classes 1 (black line) to 6 (light grey line), and for a normally maintained slab track (blue line).

The metro train running in the tunnel consists of five coaches (Fig. 3). The vehicle properties are taken from [7] and are summarized in Table 4. A 3-DOF quarter-car model including the axle (unsprung) mass, half of the bogie mass, and a quarter of the car body mass is used.

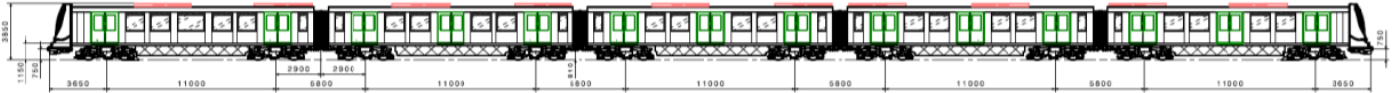


Fig. 3 Metro train with five coaches.

Table 4 Properties of the metro train.

Car body	Length	$l_v = 16.8 \text{ m}$
	Mass	$m_c = 74000 \text{ kg}$
Bogie	Bogie spacing	$l_b = 11 \text{ m}$
	Mass	$m_b = 8000 \text{ kg}$
Wheelset (unsprung mass)	Axle spacing	$l_a = 2.4 \text{ m}$
	Mass	$m_a = 1300 \text{ kg}$
Primary suspension	Vertical stiffness (per axle)	$k_1 = 3 \times 10^6 \text{ N/m}$
	Vertical viscous damping (per axle)	$c_1 = 9.5 \times 10^3 \text{ Ns/m}$
Secondary suspension	Vertical stiffness (per bogie)	$k_2 = 2.8 \times 10^6 \text{ N/m}$
	Vertical viscous damping (per bogie)	$c_2 = 80 \times 10^3 \text{ Ns/m}$

Demonstration

We will demonstrate how computations are made with the vibration prediction tool. A detailed explanation and tutorial examples are provided in [12]. First, the track geometry is defined. Since a 2.5D methodology is used, the model is restricted to straight track sections; the track and soil properties should be invariant along the track. The track properties, including the track unevenness, are selected from the database. User specified data can also be entered.

Next, the train composition is defined. This is achieved by selecting one or more carriage types from the vehicle database, which includes properties of IC trains, high speed trains, freight trains, trams and metro trains. The user can define new vehicles. The train speed is selected and wheel roughness can also be added.

A soil profile is selected from the numerical database consisting of 5 homogeneous soils (soft, moderately soft, medium, moderately stiff and stiff) and 7 layered soils (sites at Furet, Gerona, Groene Hart, Horstwalde, Ledsgard, Lincent and Steventon) [7]. The receiver distances (up to 64 m from the track) are specified by the user and the corresponding soil impedance and track-soil transfer functions are loaded from the database. Two options are available: (1) a point calculation (Fig. 4a) for individual receiver points, for which building correction factors can also be defined (small, concrete building in this case), and (2) a grid calculation (Fig. 4b). The output is given as the overall (band averaged) vibration velocity level. By selecting a receiver, the one-third octave band spectrum of the vibration velocity level is obtained in the free field (threshold), the building foundation and at mid-span of the building floor (Fig. 5).

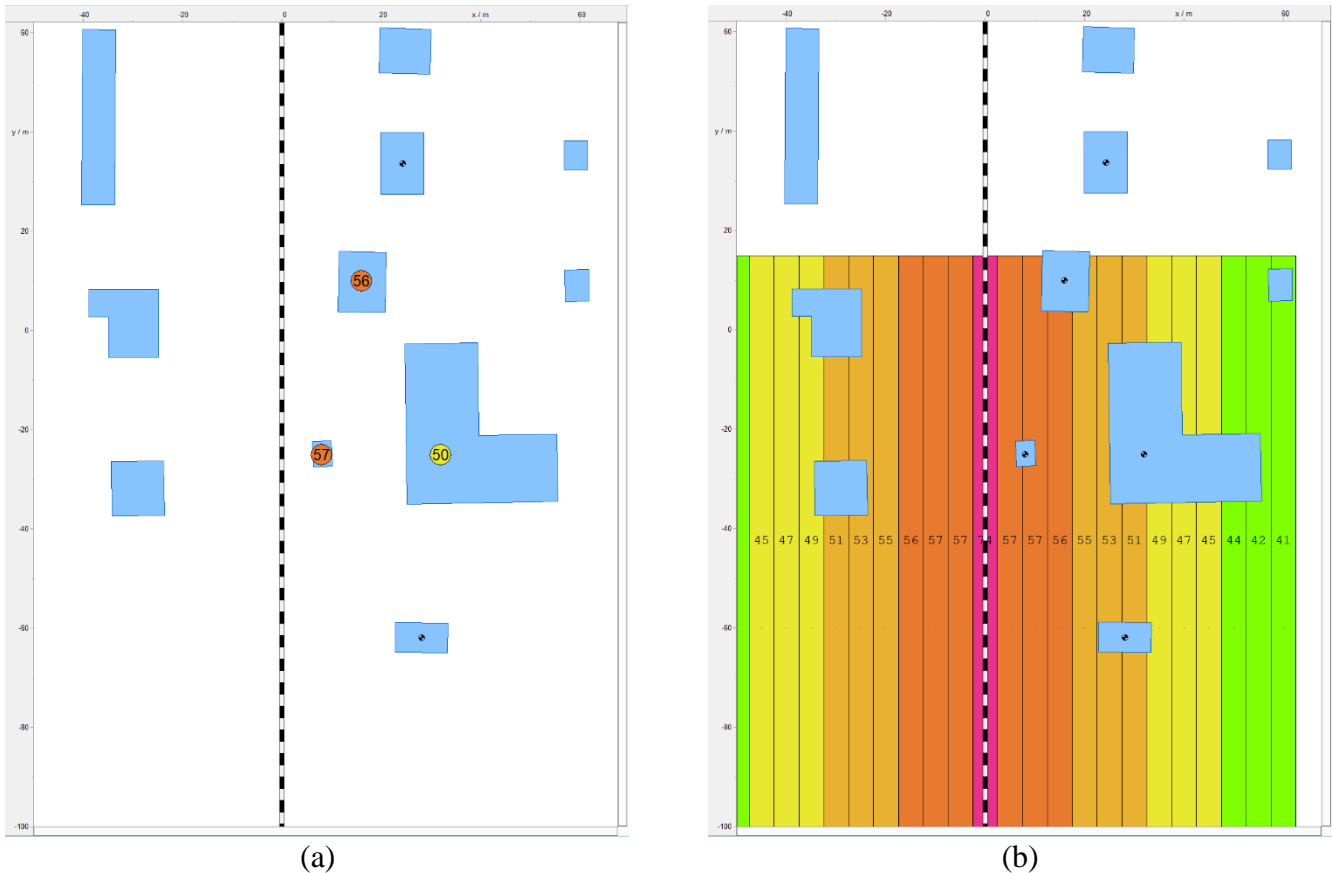


Fig. 4 Visualization of the overall (band averaged) vibration velocity levels obtained with (a) a point calculation for receivers at 8 m, 16 m and 32 m and (b) a grid calculation.

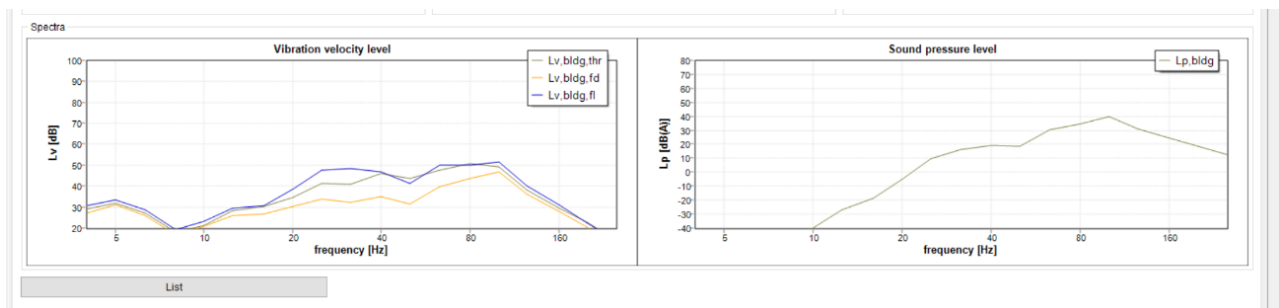


Fig. 5 One-third octave band spectrum of the vibration velocity level in the free field, at the building foundation and at mid-span of the building floor (left) and the sound pressure level inside the building for the receiver at 16 m.

Validation

Fig. 6 shows the line source transfer mobility $TM_L(\mathbf{X}, \mathbf{x}_1)$ at 16 m from the tunnel (on the free surface) embedded in soft, medium and stiff soil. It is computed with the vibration prediction tool and with MOTIV for 21 source points at the rail heads (0.5 N on each rail) with a spacing of 10 m, covering a total distance of 200 m. The results obtained with both models are in very good agreement. The narrow-band track-soil transfer functions are characterized by many peaks and dips, related to the shear and dilatational wave speed in the soil and to the distance between the tunnel invert and the receiver [13]. This is reflected in the line source transfer mobility at low frequencies; at high frequencies, individual dips and peaks cannot be observed as the results are band averaged.

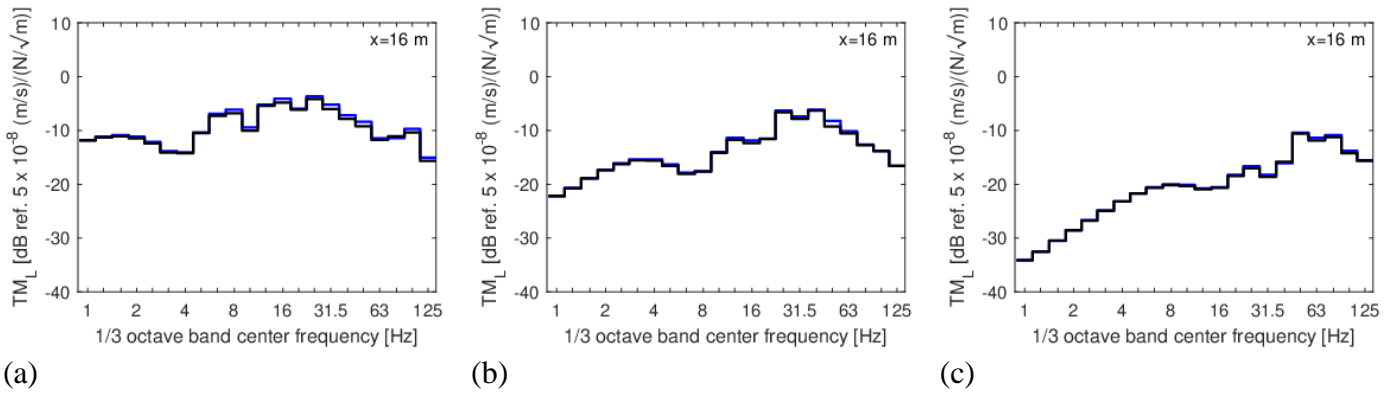


Fig. 6 Line source transfer mobility at 16 m from the tunnel embedded in (a) soft, (b) medium and (c) stiff soil. Results are computed with the vibration prediction tool (black line) and with MOTIV (blue line).

Fig. 7 shows the vibration velocity level $L_v(\mathbf{x}_1)$ during a passage of the metro train at 60 km/h in the tunnel embedded in soft, medium and stiff soil computed with the vibration prediction tool and with MOTIV. Both models use a low speed approximation, but incoherent axles are assumed in the vibration prediction tool whereas MOTIV considers coherent axles. This difference explains most of the discrepancies below 10 Hz. The peak around 5 Hz and dip around 10 Hz are attributed to the vehicle dynamics, while the peak around 80 Hz corresponds to the P2 resonance. Above 12 Hz, the results obtained with the vibration prediction tool and MOTIV are in good agreement. The vibration level is highest at the P2 resonance for the tunnel in stiff soil.

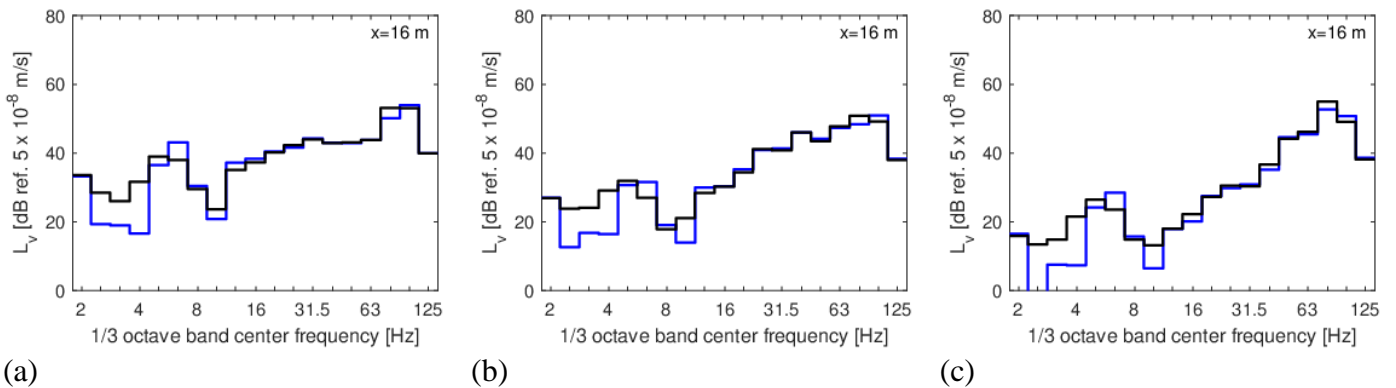


Fig. 7 Vibration velocity level at 16 m from the tunnel embedded in (a) soft, (b) medium and (c) stiff soil for the metro train running at 60 km/h. Results are computed with the vibration prediction tool (black line) and with MOTIV (blue line).

Fig. 8 shows the vibration velocity level during a train passage at 40 km/h, 60 km/h and 90 km/h in the tunnel embedded in medium soil. Good agreement between results obtained with the vibration prediction tool and MOTIV is observed for each train speed. The vibration velocity level increases in all frequency bands by about 5 dB when the train speed is increased by 50 %: as the PSD of the unevenness is proportional to k_y^{-n} with n approximately equal to 4, the amplitude of the dynamic axle loads and the vibration velocity amplitude increases by $v^{0.5(n-1)} = 1.84$ or about 5.3 dB [14].

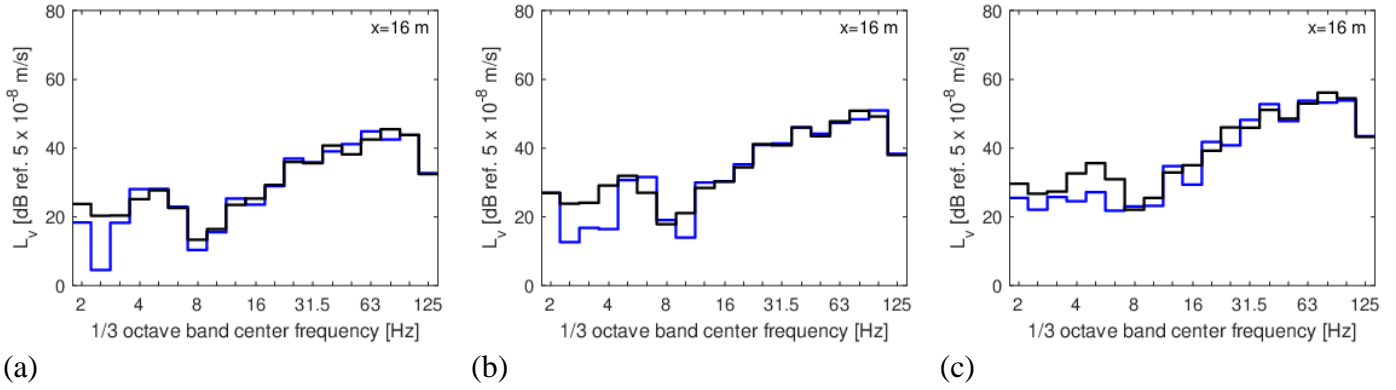


Fig. 8 Vibration velocity level at 16 m from the tunnel embedded in medium soil for the metro train running at (a) 40 km/h, (b) 60 km/h and (c) 90 km/h. Results are computed with the vibration prediction tool (black line) and with MOTIV (blue line).

The force density $L_F(\mathbf{X}, \mathbf{x}_1)$ for the tunnel embedded in soft, medium and stiff soil is shown in Fig. 9. While significant differences are observed for results obtained with the vibration prediction tool and MOTIV below 12 Hz, the discrepancy at higher frequencies is limited to 3 dB around the P2 resonance. The spectral shape is similar for each soil type, which is expected as the influence of the soil stiffness on the track compliance, and hence the dynamic axle loads, is only significant at low frequencies.

The influence of the train speed on the force density is illustrated in Fig. 10 for the tunnel embedded in medium soil: an increase of about 5 dB is found when the train speed increases by 50%. The change in force density is the same as the change in vibration velocity level, as the line source transfer mobility does not change.

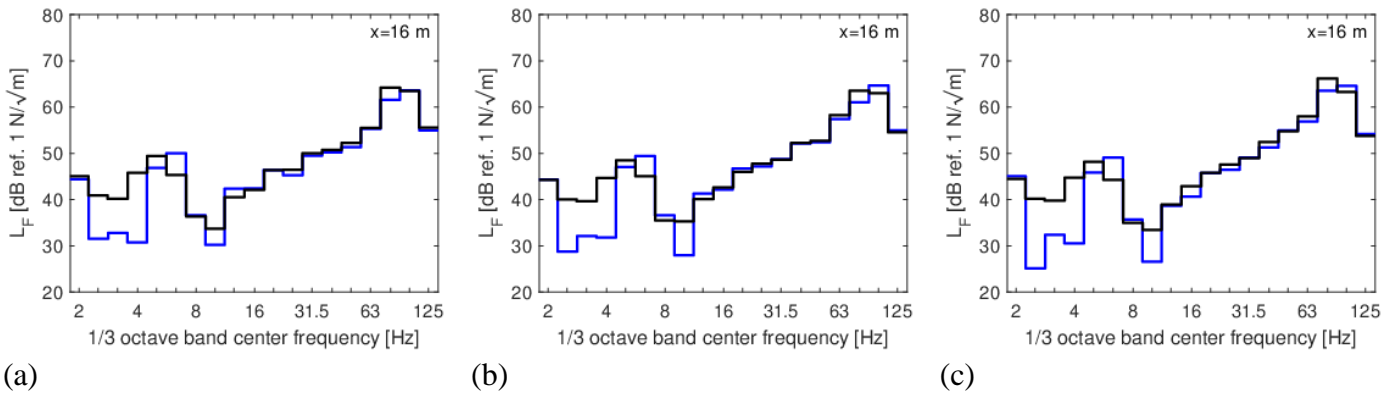


Fig. 9 Force density at 16 m from the tunnel embedded in (a) soft, (b) medium and (c) stiff soil for the metro train running at 60 km/h. Results are computed with the vibration prediction tool (black line) and with MOTIV (blue line).

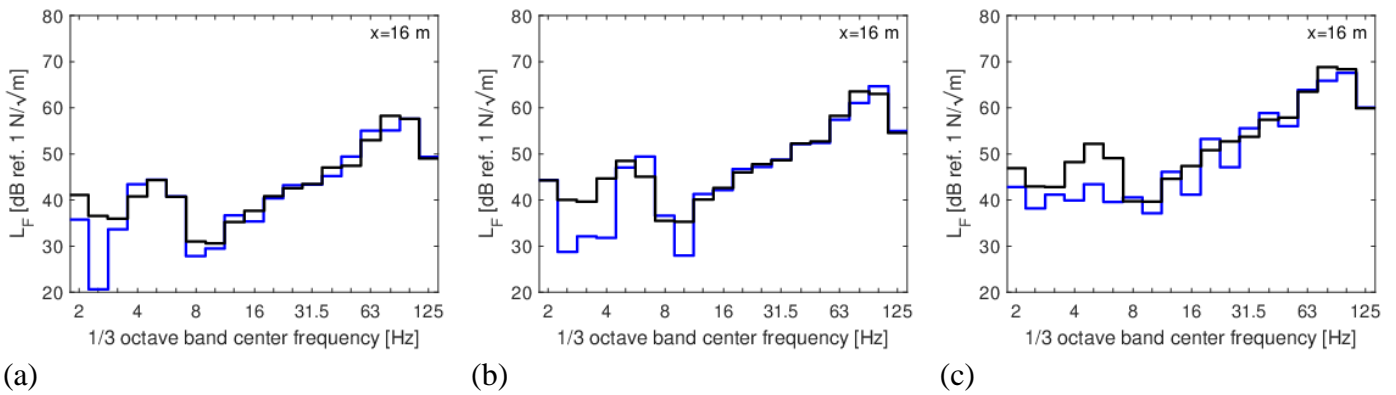


Fig. 10 Force density at 16 m from the tunnel embedded in medium soil for the metro train running at (a) 40 km/h, (b) 60 km/h and (c) 90km/h. Results are computed with the vibration prediction tool (black line) and with MOTIV (blue line).

BALLASTED TRACK IN LINCENT

The ballasted track on the high speed line L2 Brussels-Köln at a site in Lincient (Belgium) is considered in this section. Track-soil transfer functions and vibration velocity levels during passages of IC, ICE and Thalys trains were measured [15, 16]. The track and soil properties were also estimated from in situ tests. This case history is used to demonstrate and validate the hybrid prediction schemes in the vibration prediction tool.

Case description

The test site in Lincient is located next to the high speed line L2 at kilometer 61.450. The high speed railway line is constructed in a 1 m deep excavation and runs parallel to the E40 highway separated by an embankment. A cross section of the site is shown in Fig. 11. The ballasted track consists of two UIC 60 rails supported every 0.6 m by rubber pads on monoblock concrete sleepers. The track gauge equals 1.435 m. The track properties are summarized in Table 5 [3, 17].

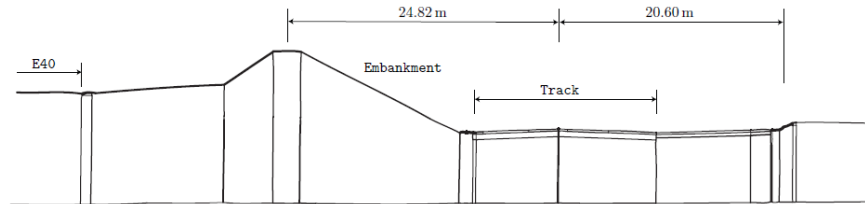


Fig. 11 Cross section of the ballast track in Lincient.

In situ tests were performed at the site in Lincient for the identification of the (small strain) dynamic soil characteristics, including Seismic Cone Penetration Tests (SCPTs), Spectral Analysis of Surface Waves (SASW) tests and Seismic Refraction (SR) tests. The results from these tests are summarized in [18]. Table 6 presents the dynamic soil characteristics at the Lincient site, which are used for the computation of the track-soil transfer functions.

The track is situated in a 1 m deep excavation. A 1 m deep lime stabilization is situated directly below the track. Verbraken [3] showed that the lime stabilization can be modeled as a 1 m stiffer top layer with estimated properties $C_s = 300$ m/s, $\nu = 1/3$ and $\rho = 1854$ kg/m³. This results in the soil layering given in Table 7, which is used for the computation of the track compliance.

Table 5 Properties of the ballasted track in Lincent.

Rail UIC60	(cfr. Table 3)	
Rail pad	Stiffness	$k_{rp} = 153.4 \times 10^6$ N/m
	Damping	$c_{rp} = 13.5 \times 10^3$ Ns/m
Sleeper	Length	$l_{slp} = 2.5$ m
	Width	$b_{slp} = 0.235$ m
	Height	$h_{slp} = 0.205$ m
	Mass	$m_{slp} = 300$ kg
	Mass moment of inertia	$\rho I_{t,slp} = 157.3$ kgm ²
	Spacing	$d = 0.6$ m
Ballast	Thickness	$h_{bal} = 0.35$ m
	Top width	$b_{balt} = 3.6$ m
	Bottom width	$b_{balb} = 5.6$ m
	Mass per unit length	$m_{bal} = 1488$ kg/m
	Stiffness per sleeper	$k_{bal} = 180 \times 10^6$ N/m
	Damping loss factor	$\eta_{bal} = 0.06$

Table 6 Dynamic soil characteristics at the Lincent site.

Layer	Thickness [m]	C_s [m/s]	C_p [m/s]	ρ [kg/m ³]	β_s [-]	β_p [-]
1	1.4	128	286	1800	0.044	0.044
2	2.7	176	286	1800	0.038	0.038
3	∞	355	1667	1800	0.037	0.037

Table 7 Dynamic soil characteristics for the computation of the track compliance, accounting for the 1 m deep excavation and 1 m thick lime stabilization below the track at the Lincent site.

Layer	Thickness [m]	C_s [m/s]	C_p [m/s]	ρ [kg/m ³]	β_s [-]	β_p [-]
1	1.0	300	600	1854	0.044	0.044
2	2.1	176	286	1800	0.038	0.038
3	∞	355	1667	1800	0.037	0.037

Four different train types are operating on the line L2 in Lincent: the InterCity (IC) trains of type IC-A and IC-O, and the Thalys and ICE high speed trains. The train speed for the IC trains varies between 160 km/h to 214 km/h. The Thalys train runs at 300 km/h.

We consider passages of the Thalys train, which consists of 2 locomotives, one at each end of the train, and 8 carriages in between (articulated composition). The total length equals 200.19 m from first to last axle. The total number of bogies is 13 and, consequently, the total number of axles is 26. The vehicle properties are summarized in Table 8.

Table 8 Properties of the Thalys train: vehicle length l_v , bogie spacing l_b , axle spacing l_a , total mass per axle m_t , sprung mass m_s and unsprung mass m_u .

	Number of axles	l_v [m]	l_b [m]	l_a [m]	m_t [kg]	m_s [kg]	m_u [kg]
Locomotive	4	22.15	14.00	3.00	17000	14973	2027
Side carriage	3	21.84	18.70	3.00	17000	14973	2027
Central carriage	2	18.70	18.70	3.00	17000	14973	2027

The Belgian railway infrastructure manager Infrabel used the EM130 measurement vehicle equipped with an Applanix POS/TG system to record the irregularity and alignment of both rails and the curvature, superelevation and grade of the track. The track unevenness at the Lincent site was measured on the track in the direction of Liège in April 2011. From these measurements, the PSD of the average vertical unevenness of both rails was computed. It is reliable in a wavelength range between 3 m and 63 m. The unevenness for smaller and larger wavelengths was extrapolated from the measurements by fitting the PSD to the analytical formula proposed by the FRA. The measured and fitted PSD are shown in Fig. 12, together with the FRA curves (classes 1 to 6).

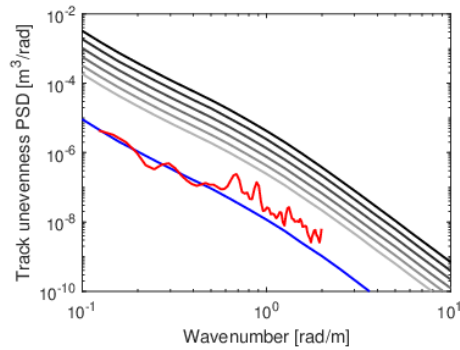


Fig. 12 One-sided PSD of the track unevenness for FRA track quality classes 1 (black line) to 6 (light grey line), measured unevenness at the site in Lincent (red line) and estimated fit (blue line).

Demonstration

For the Lincent site, the GIS software Open Street Map is used to define the track geometry. The position of the track is selected on the map and the location of the receiver points is specified (Fig. 13). If present, any nearby buildings could also be selected as receiver locations; a building type has to be specified in order to select appropriate building correction factors. The track, soil and vehicle properties, as well as the track unevenness are defined by the user.

When performing hybrid computations, the user needs to enter empirical data for either the force density or the line source transfer mobility (one-third octave band spectra).

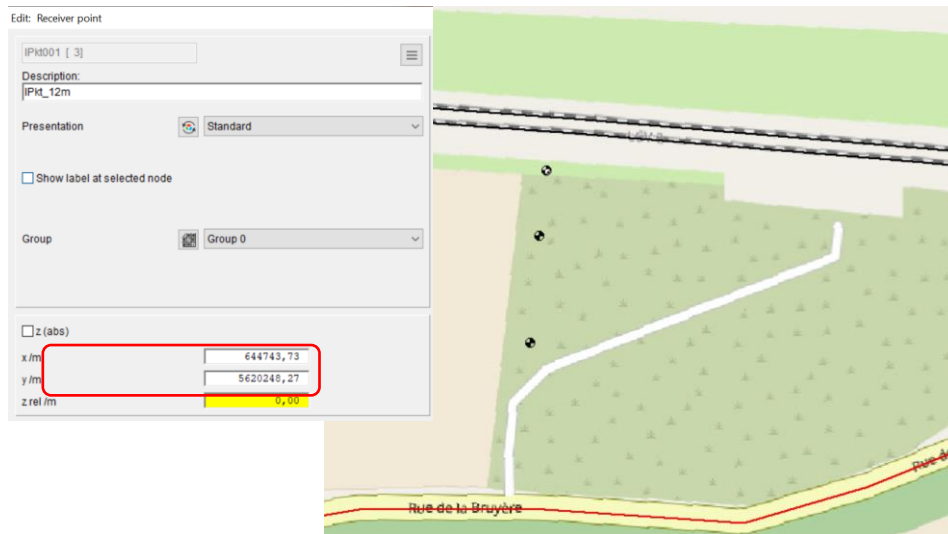


Fig. 13 The Lincent site in Open Street Map and definition of receiver points.

Validation

The line source transfer mobility at the site in Lincent was measured by applying hammer impacts at the sleeper edge every 10m along the track, covering a total distance of 200 m [3]. Numerical predictions of the line source transfer mobility are made with the vibration prediction tool and TRAFFIC [10]; 21 source points are considered at the rail heads (0.5 N on each rail) every 10 m covering a total distance of 200 m.

Fig. 14 shows the line source transfer mobility $TM_L(\mathbf{X}, \mathbf{x}_1)$ at 12 m, 32 m and 64 m from the track. The measured data show a significant amount of noise below 8 Hz. At higher frequencies, the predicted and measured line source transfer mobility match relatively well for the receivers at 12 m and 32 m. At 64 m, relatively good correspondence is observed between 10 Hz and 30 Hz, while at higher frequencies the predictions are around 15 dB below the measured results. This is attributed to uncertainty on the estimated soil properties, particularly the material damping ratios, and to the different impact location in the experiment (on the sleeper edge) and the predictions (on both rail heads). To account for the different impact location, the measured line source transfer mobility has been modified by application of a correction factor $\Delta TM_L(\mathbf{X}, \mathbf{x}_1)$, which is computed with the numerical prediction scheme; the corrected, experimental line source transfer mobility is used in the hybrid prediction schemes. The predictions of the line source transfer mobility with the vibration prediction tool and TRAFFIC are in excellent agreement across the entire frequency range.

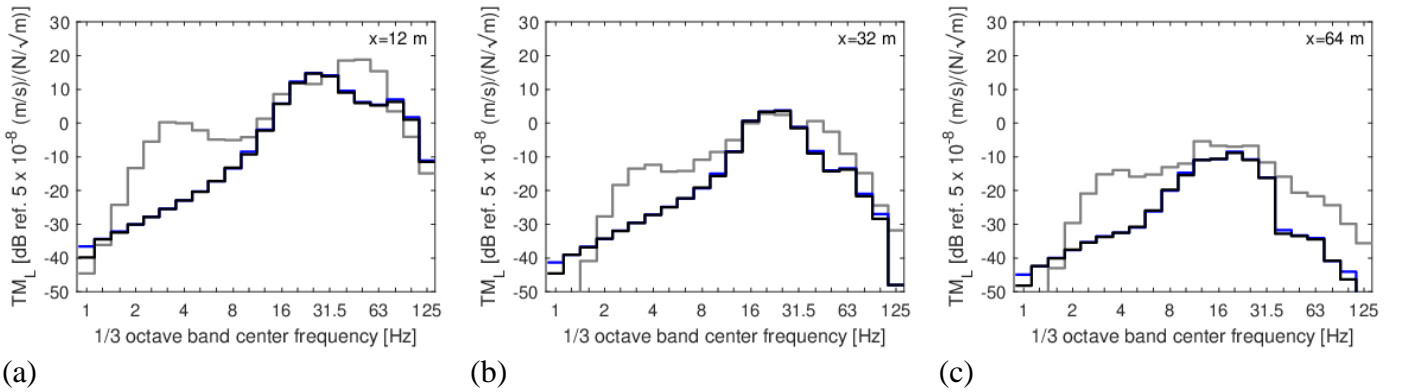


Fig. 14 Line source transfer mobility for the ballasted track in Lincent. Receivers are located at (a) 12 m, (b) 32 m and (c) 64 m from the track. Measured data (grey line) are compared to results computed with the vibration prediction tool (black line) and with TRAFFIC (blue line).

Fig. 15 shows the vibration velocity level $L_v(\mathbf{x}_1)$ at 12 m, 32 m and 64 m from the track during the passage of the Thalys train at 292 km/h. The vibration velocity level is predicted with hybrid schemes 1 and 2 (Eqs. 2b and 3, respectively), and with two models in TRAFFIC: a detailed model accounting for the Doppler effect, and a simplified model in which identical assumptions as in the vibration prediction tool (low speed approximation and incoherent axle loads) are made. The vibration velocity level was also measured during five train passages.

The predictions with hybrid scheme 1 show good agreement with the measured data at low frequencies. However, this is not expected since the contribution of the quasi-static axle loads is not included in the predicted vibration velocity level $L_v^{NUM}(\mathbf{x}_1)$ in Eq. 2b. Instead, this is explained by the low-frequency noise on the measured line source transfer mobility $TM_L^{EXP}(\mathbf{X}, \mathbf{x}_1)$ (Fig. 14). An overestimation of the vibration velocity level is observed around the P2 resonance (between 50 Hz and 60 Hz). At 32 m and 64 m, the predicted and measured vibration levels match better at high frequencies compared to the fully numerical predictions with TRAFFIC, due to the use of the measured line source transfer mobility.

For hybrid scheme 2, the discrepancy at low frequencies is not expected since the contribution of the quasistatic axle loads is, of course, included in the measured vibration velocity level $L_v^{EXP}(\mathbf{x}_1)$ in Eq. (3). This contribution is, however, cancelled out by the low-frequency measurement noise on the measured line source transfer

mobility $TM_L^{EXP}(\mathbf{X}, \mathbf{x}_1)$. The use of hybrid scheme 2 results in a good prediction of the vibration velocity level between 10 Hz and 60 Hz for the receivers at 12 m and 32 m; the spectrum clearly shows the peak around 25 Hz corresponding to the axle passage frequency. At higher frequencies, however, hybrid scheme 2 suffers from the uncertainty on the dynamic soil characteristics used for the prediction of the line source transfer mobility $TM_L^{NUM}(\mathbf{X}, \mathbf{x}_1)$, and therefore underestimates the vibration velocity level at 32 m and 64 m from the track.

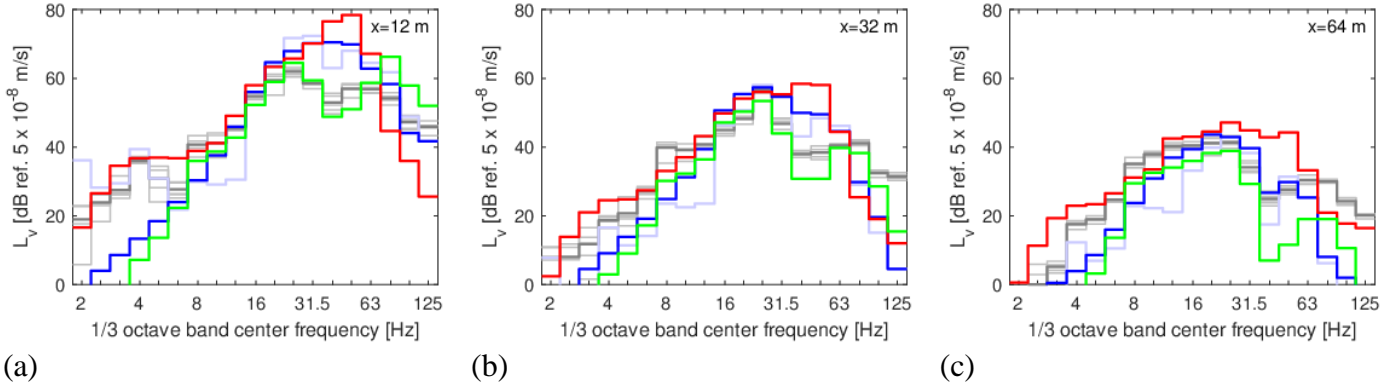


Fig. 15 Vibration velocity level during the passage of the Thalys train running at 292 km/h on the ballasted track in Lincet. Receivers are located at (a) 12 m, (b) 32 m and (c) 64 m from the track. Results are computed with the vibration prediction tool using hybrid prediction schemes 1 (red line) and 2 (green line), and with the detailed model (light blue line) and simplified model (dark blue line) in TRAFFIC. The five measured train passages are also shown (light grey lines) as well as their average (dark grey line).

CONCLUSIONS

This paper presents the hybrid vibration prediction tool for railway induced vibration developed within the project SILVARSTAR. The hybrid framework is outlined and two case histories are used for demonstration and validation: a slab track in a tunnel and a ballast track at grade in Lincet (Belgium). Results obtained with the fully numerical prediction scheme are in very good agreement with those obtained with state-of-the-art models. This validates the computational core of the vibration prediction tool. The case history in Lincet is used to demonstrate the hybrid prediction schemes. Overall, reasonable agreement between the hybrid predictions and measured data is obtained, particularly when the experimental force density is used (hybrid scheme 2).

ACKNOWLEDGEMENTS

This paper is the result of the project SILVARSTAR funded from the Shift2Rail Joint Undertaking under the European Union's Horizon 2020 Research and Innovation Programme under Grant Agreement 101015442. This financial support is gratefully acknowledged.

DISCLAIMER

The information in this document is provided "as is", and no guarantee or warranty is given that the information is fit for any particular purpose. The content of this document reflects only the authors' view - the Shift2Rail Joint Undertaking is not responsible for any use that may be made of the information it contains. The users use the information at their sole risk and liability.

REFERENCES

- [1] C. E. Hanson, J. C. Ross and D. A. Towers, "High-Speed Ground Transportation Noise and Vibration Impact Assessment," Technical Report DOT/FRA/ORD-12/15, U.S. Department of Transportation, Federal Railroad Administration, Office of Railroad Policy and Development, September 2012.

- [2] A. Quagliata, M. Ahearn, E. Boeker, C. Roof, L. Meister and H. Singleton, "Transit Noise and Vibration Impact Assessment Manual," FTA 0123, U.S. Department of Transportation, Federal Transit Administration, John A. Volpe National Transportation Systems Center, September 2018.
- [3] H. Verbraken, "Prediction of railway induced vibration by means of numerical, empirical, and hybrid methods," PhD thesis, Department of Civil Engineering, KU Leuven, 2013.
- [4] P. Reumers, G. Degrande, G. Lombaert, F. Seyfaddini, G. Herremans, E. Ntotsios, D. J. Thompson, B. Nélain, P. Bouvet, B. Fröhling and A. Nuber, "Validation of the prototype vibration prediction tool against documented cases," SILVARSTAR project GA 101015442, Deliverable D1.3, Report to the EC, June 2022.
- [5] X. Sheng, C. J. C. Jones and D. J. Thompson, "Prediction of ground vibration from trains using the wavenumber finite and boundary element methods," *Journal of Sound and Vibration*, vol. 293, p. 575–586, 2006.
- [6] S. François, M. Schevenels, G. Degrande, G. Lombaert and P. Galvín, "A 2.5D coupled FE-BE methodology for the dynamic interaction between longitudinally invariant structures and the soil," in *Proceedings of COMPDYN 2009, 2nd International Conference on Computational Methods in Structural Dynamics and Earthquake Engineering*, Rhodes, 2009.
- [7] D. J. Thompson, E. Ntotsios, G. Degrande, G. Lombaert, G. Herremans, T. Alexiou, B. Nélain, S. Barcet, P. Bouvet, B. Fröhling and A. Nuber, "Database for vibration emission, ground transmission and building transfer functions," SILVARSTAR project GA 101015442, Deliverable D2.1, Report to the EC, February 2023.
- [8] X. Sheng, C. J. C. Jones and D. J. Thompson, "A theoretical model for ground vibration from trains generated by vertical track irregularities," *Journal of Sound and Vibration*, vol. 272, pp. 937-965, 2004.
- [9] E. Ntotsios, D. J. Thompson and M. F. M. Hussein, "A comparison of ground vibration due to ballasted and slab tracks," *Transportation Geotechnics*, vol. 21, 2019.
- [10] G. Lombaert, S. François and G. Degrande, "TRAFFIC Matlab toolbox for traffic induced vibrations," Report BWM-2011-12, Department of Civil Engineering, KU Leuven, March 2012.
- [11] P. Reumers, G. Degrande, G. Lombaert, B. Nélain, P. Bouvet, B. Fröhling, A. Nuber, E. Ntotsios and D. J. Thompson, "Report on approval testing," SILVARSTAR project GA 101015442, Deliverable D3.3, Report to the EC, February 2023.
- [12] Nuber A., J. Schrauth, B. Fröhling, B. Nélain and P. Bouvet, "Ground vibration prediction software: user's manual and tutorial examples," SILVARSTAR project GA 101015442, Deliverable D3.2, Report to the EC, February 2023.
- [13] S. Gupta, M. F. M. Hussein, G. Degrande, H. E. M. Hunt and D. Clouteau, "A comparison of two numerical models for the prediction of vibrations from underground railway traffic," *Soil Dynamics and Earthquake Engineering*, vol. 27, p. 608–624, 2007.
- [14] G. Lombaert and G. Degrande, "Ground-borne vibration due to static and dynamic axle loads of InterCity and high speed trains," *Journal of Sound and Vibration*, vol. 319, pp. 1036-1066, 2009.
- [15] H. Verbraken, P. Coulier, G. Lombaert and G. Degrande, "Measurement of train passages and transfer functions at a site in Lincent," Report BWM-2012-05, Department of Civil Engineering, KU Leuven, June 2012.
- [16] H. Verbraken, P. Coulier, G. Lombaert and G. Degrande, "Measurement of transfer functions at a site in Lincent," Report BWM-2012-07, Department of Civil Engineering, KU Leuven, July 2012.
- [17] G. Lombaert, G. Degrande, J. Kogut and S. François, "The experimental validation of a numerical model for the prediction of railway induced vibrations," *Journal of Sound and Vibration*, vol. 297, pp. 512-535, 2006.

[18] H. Verbraken, G. Degrande, G. Lombaert, B. Stallaert and V. Cuéllar, "Benchmark tests for soil properties, including recommendations for standards and guidelines," RIVAS project SCP0-GA-2010-265754, Deliverable D1.11, Report to the EC, December 2013.